

Title no. 95-S47

Seismic Response of Precast Concrete Frames with Hybrid Connections



by G. S. Cheek, W. C. Stone, and S. K. Kunnath

The analytically simulated performance of moment-resisting precast concrete frames with hybrid connections under seismic loads is evaluated. An enhanced and versatile hysteretic model was developed to represent the inelastic behavior of the hybrid precast connection region. The model parameters were calibrated using results from a separate experimental program which examined the inelastic cyclic behavior of hybrid concrete precast connections. An interesting feature of the connection was the hybrid combination of mild steel and post-tensioning or post-tensioning steel where the mild steel was used to dissipate energy by yielding and the post-tensioning steel was used to provide the shear resistance through friction developed at the beam-column interface. To simulate the seismic response of actual buildings constructed with such hybrid precast connections, a series of two-dimensional structural models representing typical four, eight, twelve, and twenty-two story precast frames was subjected to a series of earthquake motions. The analyses included 29 different accelerograms, representing all three UBC soil types, and were scaled to fit the UBC design spectra. Results of the inelastic dynamic analyses are used in conjunction with experimental results to develop simple design guidelines for the use of precast concrete hybrid connections in regions of high seismicity.

Keywords: analytical modeling; beam-column frame; building technology; concrete; hysteresis model; joints (connections); moment resisting; post-tensioning; precast.

INTRODUCTION

The potential benefits of precast concrete in terms of construction speed, efficiency, and quality control are well recognized. However, its use in high seismic zones has been impeded by the lack of test data on the performance, ductility, and energy-dissipation capacity of such connections. An extensive series of tests completed recently at the National Institute of Standards and Technology (NIST) (Stone et al. [1995]) has provided important information on the inelastic cyclic behavior of hybrid precast concrete connections. The objective of this study is to use the experimentally measured force-deformation behavior and apply it in an extensive parametric study of regular precast frame structures under the action of earthquake forces in regions of high seismicity. The results of the evaluation are expected to provide preliminary information on the seismic adequacy of such connections for use in Seismic Zone 4 construction.

The analyses were conducted using IDARC, a computer program for inelastic damage analysis of reinforced concrete

structures (IDARC) (Kunnath et al. [1992]). The primary objective of the study was to determine the inelastic dynamic behavior of a frame structure constructed with hybrid precast concrete connections. A new hysteretic model was developed using the observed hysteresis behavior data, and incorporated into IDARC to facilitate a detailed nonlinear seismic evaluation of precast frame structures with hybrid connections. The results of the dynamic analyses were used in conjunction with the experimental results to develop design guidelines for precast concrete hybrid connections in regions of high seismicity.

RESEARCH SIGNIFICANCE

The use of precast concrete in regions of high seismicity has been hindered by the lack of data on the potential seismic performance of such connections. The results of this study will contribute significantly to the much-needed database of knowledge on the expected performance of precast concrete structures subjected to severe earthquake loading. The proposed drift demands, based on soil-type, as presented in this paper can be perceived as a first step in developing simplified design guidelines for the use of precast connections in high seismic zones. The analytical procedures used in this paper may also be viewed as a methodology for the transfer of experimental results to the development of design criteria.

BACKGROUND

A brief summary of the experimental phase of this project is presented. An extensive testing program to study the seismic performance of $1/3$ -scale precast concrete beam-column connections was conducted at NIST (Cheek and Lew [1991, 1993]; Cheek and Stone [1993, 1994]). The objective of the program was to develop recommended guidelines for precast beam-column connections in regions of high seismic activi-

ACI Structural Journal, V. 95, No. 5, September-October 1998.

Received December 10, 1996, and reviewed under Institute publication policies. Copyright © 1998, American Concrete Institute. All rights reserved, including the making of copies unless permission is obtained from the copyright proprietors. Pertinent discussion will be published in the July-August 1999 ACI Structural Journal if received by March 1, 1999.

ACI member G. S. Cheok is research structural engineer at the National Institute of Standards and Technology, Gaithersburg, MD. She obtained her BS and MS degrees from the University of Maryland, and is currently active in research on seismic behavior of precast concrete structures.

W. C. Stone is research structural engineer at the National Institute of Standards and Technology, Gaithersburg, MD. He obtained his BS and MS from Rensselaer Polytechnic Institute and his PhD from the University of Texas at Austin. His research interests include structural dynamics, real-time metrology, and robotics and automation in construction.

ACI member S. K. Kunnath is associate professor at the University of Central Florida, Orlando, FL. He received his MEng from the Asian Institute of Technology and his PhD from the State University of New York at Buffalo. He is involved in research on nonlinear modeling and seismic damage assessment of concrete and steel reinforced concrete structures.

ty. The basic concept for the connection design was that its shear resistance was provided by the friction developed between the beam-column interface from the post-tensioning force, thus eliminating the need for corbels or shear keys.

A total of 22 specimens were tested. Of the 22 specimens, four were monolithic specimens used as benchmark tests for the precast connections. The most promising precast connection was a hybrid design (Specimen OPZ4) which consisted of mild steel ($f_y = 414$ MPa [60 ksi]) and post-tensioning or post-tensioning (PT) steel ($f_u = 1862$ MPa [270 ksi]). The mild steel was used to dissipate energy by yielding and the PT steel was used to provide the shear resistance through friction developed at the beam-column interface. Therefore, to maintain the required shear resistance, it was necessary for the PT steel to remain elastic throughout the expected range of displacement.

The mild steel was fully bonded, except for 25 mm (1 in.) on either side of the beam-column interface, and was located at the top and bottom of the beam. The mild steel was unbonded over a short length (25 mm [1 in.]) to delay fracture of the bars. Earlier tests showed that premature bar fracture led to failure of the specimen shortly thereafter. The post-tensioning steel was partially bonded and located at mid-depth of the beam. The unbonded length and the location of the post-tensioning steel allowed the specimens to achieve story drifts of 4 percent before yielding of the post-tensioning steel occurred. Since the test specimens failed at story drifts of 3 percent to 3.5 percent, this meant that the PT steel remained in the elastic range through failure. A typical precast frame composed of hybrid connections and the basic connection details at the joint region are shown in Fig. 1.

The performance of the hybrid connections was shown to be comparable to that for a monolithic connection in terms of strength, drift capacity, and energy dissipation. However, the hybrid connections were superior in two important aspects: the connections sustained significantly less damage than the monolithic connections; and the connections were self-centering with essentially no residual drift following large inelastic deformations. More detailed descriptions of the test program and observations may be found in Stone et al. (1995), Cheok and Stone (1993, 1994), Cheok and Lew (1993), and Cheok and Lew (1991). Similar investigations, involving different assembly schemes, have been performed (Priestley [1994]; French [1989a, 1989b]).

ANALYTICAL MODELING

An investigation of the seismic performance of the precast frame system was carried out using the nonlinear analysis program IDARC. Recent studies (Kunnath and Reinhorn [1995]) have shown that IDARC is capable of adequately reproducing experimentally observed response of concrete structures in the inelastic range. However, the existing three-parameter hysteretic model in IDARC was found to be inadequate to characterize the observed force-deformation response of hybrid precast connections. Therefore, the model was enhanced to incorporate certain unique features of the experimentally observed behavior. The new model is characterized by seven parameters, the details of which are summarized in the next section.

Enhanced hysteresis model

Three primary degrading characteristics are identified in the experimental force-deformation loops: stiffness degradation, strength deterioration, and pinching. It was determined that a total of seven parameters were required to characterize adequately all essential aspects of the observed behavior. These seven parameters are defined in conjunction with a trilinear moment-curvature envelope as shown in Fig. 2; and explained below.

Stiffness degradation—The observed force-deformation loops indicate that stiffness degradation is best expressed as a function of attained ductility. While the degradation is not obvious at small ductilities, the reduction in stiffness is more evident at larger drifts. To model the reduced stiffness, all unloading branches were directed toward a common target point as shown in Fig. 2(a). The instantaneous stiffness is given by:

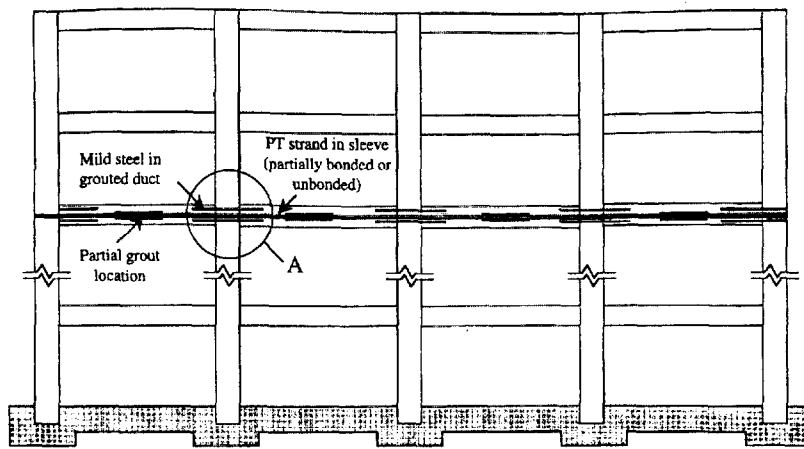
$$k^* = \frac{(M_{max} - \alpha M_y)}{(\phi_{max} - \alpha M_y/k)} \quad (1)$$

where M_{max} and ϕ_{max} are the moment and curvature values, respectively, at the start of the current unloading cycle; α is a control parameter which determines the amount of stiffness degradation; M_y is the yield moment; and k is the initial flexural rigidity (EI) of the section.

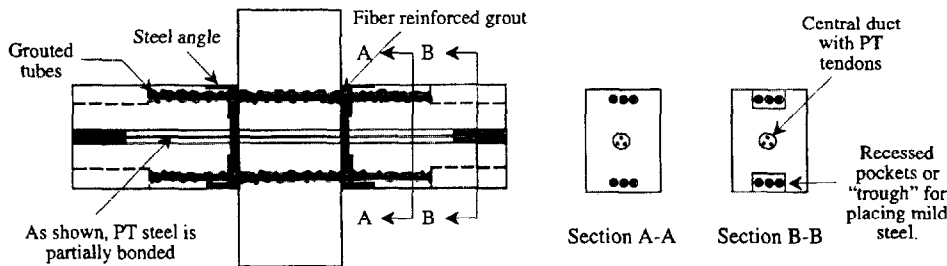
Strength deterioration—The modeling of strength decay is accomplished using four control parameters. The relative loss of strength per inelastic cycle is determined as a function of ductility and dissipated hysteretic energy. Figure 2(b) shows the modeling of strength decay, in which the following expression is used:

$$M^* = M_m(1 - \beta_E E_T - \beta_d \mu) \quad (2)$$

where M^* is the reduced strength level at the same deformation corresponding to the previous peak moment M_m , and β_E and β_d are control parameters which specify the rate of degradation in terms of dissipated hysteretic energy per cycle E_T and curvature ductility μ . The choice of two such control parameters permits more flexibility in attaining varying degrees of degradation. Reloading paths now aim for M^* instead of the previous maximum moment M_m resulting in a



Elevation



Note: Column bars omitted for clarity

Detail A

Fig. 1—Connection details for hybrid precast connections

degraded loop. Experimental observation further indicates the need for two additional control parameters which control the post-yield envelope. The first is required to degrade the post-yield stiffness further upon reaching ϕ_m by prescribing a new stiffness as follows:

$$\bar{k} = k' \frac{\eta}{\mu} \leq k' \quad (3)$$

where \bar{k} is the new stiffness upon attaining the reduced strength M^* and has a limiting value of the current instantaneous stiffness, k' , which is the post-yield stiffness of the primary envelope curve; η is a control parameter to stipulate the level of reduction in the slope of the current path; and μ is the attained curvature ductility. It is observed from the above expression that a large value of η will retain the current instantaneous stiffness and the branch will continue unchanged until the primary envelope is reached. Figure 2(b) shows the effect of introducing this parameter.

An additional parameter was introduced to redirect the loading path to intersect the primary envelope before the previous maximum point, as displayed in Fig. 2(c). The new location was prescribed as:

$$\phi_{m^*} = \xi \phi_m \quad (4)$$

where ξ is a control parameter to specify the change in stiffness to reflect the behavior shown in the figure. The effect of introducing this parameter was to marginally increase the dissipated hysteretic energy per loop.

Slip and pinching behavior—Another important characteristic of the observed hysteresis loops was the pronounced pinching behavior caused either by opening and closing of cracks or by debonding of the mild steel. Three additional parameters were prescribed to model this behavior accurately, and are shown in Fig. 2(d). During unloading (or reloading, as the case may be), when the load-deformation path crosses the slip axis, a new target point is specified as follows:

$$M^* = \gamma M_y \quad (5)$$

where γ is a control parameter which specifies the level of pinching as a function of the yield moment M_y . The slip axis is defined by a line which intersects the origin and is specified in terms of a parameter λ_1 which expresses the slope of

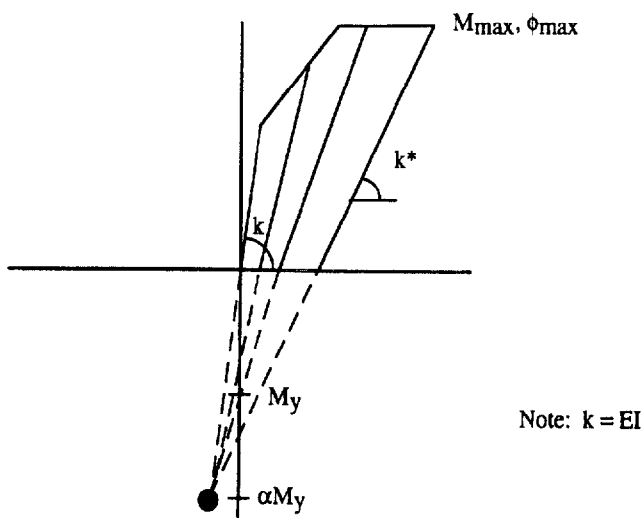


Fig. 2(a)—Hysteretic parameters: stiffness degradation

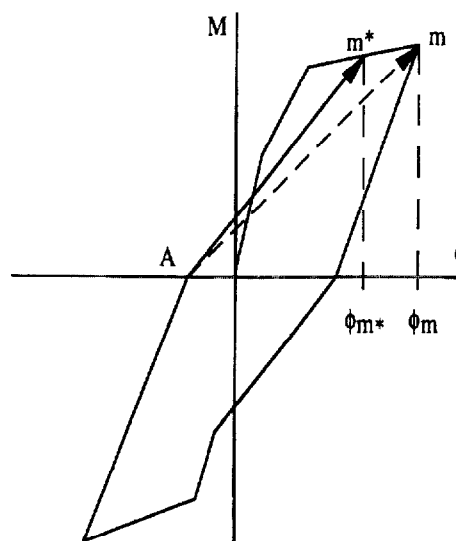


Fig. 2(c)—Hysteretic parameters: energy

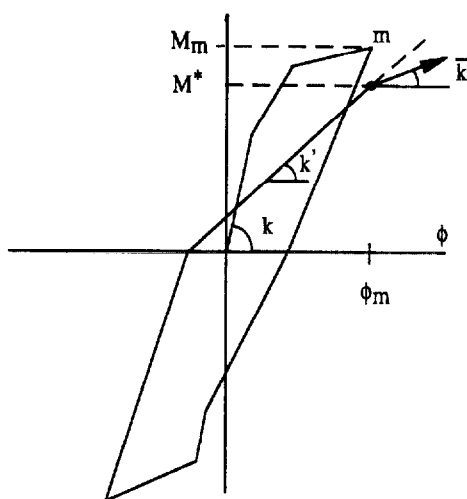


Fig. 2(b)—Hysteretic parameters: strength deterioration

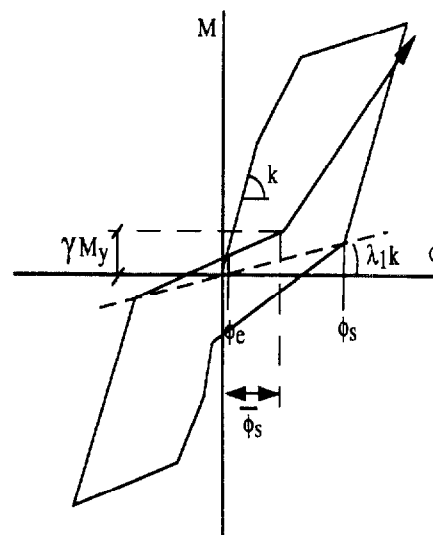


Fig. 2(d)—Hysteretic parameters: slip control

the line as a function of the initial flexural stiffness. Finally, the length of the slip zone was modeled as follows:

$$\bar{\phi}_s = \lambda_2(\phi_s - \phi_e) \quad (6)$$

where ϕ_s is the deformation level upon crossing the slip axis during the previous unloading (or reloading), ϕ_e is the deformation level corresponding to the intersection of the current branch with the initial stiffness line, and λ_2 is a user specified parameter to control the length of slip.

Identification of hysteretic parameters

The seven control parameters used in the analytical simulation were obtained from a separate identification study in which an interactive graphics program (NIDENT7) developed at NIST was used to tune the model to fit observed experimental behavior. This program allows the user to visually observe the effects of changing one or more parameters. In all, hysteretic parameters were identified for five

different connection types. The parameters were calibrated using the experimental load-deformation data which was scaled using similitude requirements to account for the reduced scale of the test specimens. The final selection of the parameters was based on minimizing the error between the predicted energy dissipated per cycle and the experimental energy dissipated per cycle.

The simulation of a typical set of force-deformation hysteresis for one of the specimens is shown in Fig. 3 which compares analytically simulated vs. experimental loops. It is seen that the model captures with sufficient accuracy the shape and degradation of the observed behavior. In general it was observed that the simulated loops slightly underpredict

Table 1—IDARC hysteretic failure parameters

Connection type (M_s/M_p)	α	β	γ	λ_1	λ_2	η	ζ
0.00 (GPZ4)	1.6	0.200	0.000	0.464	0.041	21.0	1.00
0.28 (KPZ4)	1.6	0.200	0.012	0.464	0.000	21.0	1.00
0.35 (MPZ4)	10.0	0.083	0.260	0.120	0.053	2.9	0.83
0.45 (OPZ4)	6.0	0.058	0.352	0.000	0.0076	3.2	1.00
1.00 (Monolithic)	10.0	0.200	0.480	0.150	0.004	3.0	0.95

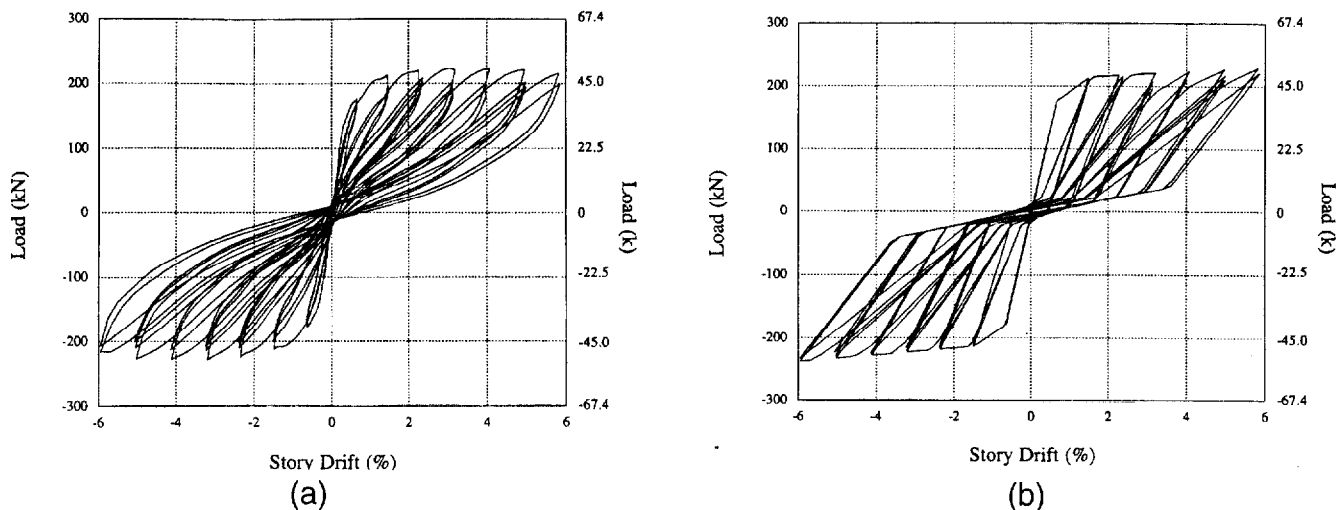


Fig. 3—Experimental vs. predicted hysteresis loops using 7-parameter model: (a) experimental (Specimen GPZ4); (b) predicted

energy at low drifts and slightly overpredict the amount of dissipated energy at higher drifts. The overall margin of error in computed vs. observed hysteretic energy for all specimens was less than ± 5 percent.

The hysteretic failure parameters resulting from the identification study for all connection types are given in Table 1.

PARAMETRIC STUDY

The revised computer program with the seven-parameter hysteresis model was used in a detailed parametric evaluation of precast structures ranging in height from four to twenty-two stories. The purpose of the evaluation was to establish expected maximum interstory drift demands and to compare them with the laboratory performance of the monolithic and hybrid precast specimens. The effects of secondary moments due to interstory drift (P-delta moments) were not investigated in this study.

Of the five precast connections tested, the hybrid connection, Specimen OPZ4 (see Stone et al. [1995] and Table 1), performed the best and is being recommended as a suitable connection type for high seismic zones. Most of the results presented on the building response pertains to this connection only, unless otherwise noted in the figure or discussion.

Description of prototype structures

Two sets of design forces were calculated for “typical” monolithic prototype buildings: one set (Table 2[b]) was provided by a design firm, and the other set (Table 2[a]) was generated in-house. Both sets of designs were based on the guidelines specified in the Uniform Building Code (1994). The dynamic models were based on a prototype building

with a floor plan of 65.8×32.9 m (216×108 ft). The structure has a perimeter frame with four bays per frame in both directions. The building weight per floor was computed assuming a uniform floor load, dead load plus live load, of 7660 Pa (160 psf). The story height was 3.96 m (13 ft). The building was designed for UBC seismic zone 4 for S1, S2, and S3 soil types. Prototype structures having 4, 8, 12, and 22 floors were studied. The design shear force in the frame was increased by 5 percent to account for accidental torsion as required by UBC provisions. The design beam moments for the prototype buildings are given in Tables 2(a) and 2(b).

Nonlinear system properties

There are two main input requirements for the program IDARC: a trilinear $M-\phi$ envelope for each beam and column cross section where inelastic action is expected to occur, and the seven parameters for the hysteretic failure model. The identification of the hysteretic parameters was described in the previous section. The specification of the $M-\phi$ envelope presented a more formidable task since there is currently no available procedure to construct the monotonic moment vs. curvature envelope for a hybrid precast connection. A procedure was, therefore, developed to generate the required trilinear envelope from the “reference” moments given in Table 2 for monolithic connections. The initial stiffness was based on the prototype beam dimensions, and the yield moment for the section was set equal to the design beam moment for that floor. The remaining parameters to complete the $M-\phi$ envelope were developed by maintaining simi-

Table 2(a)—Prototype beam moments: Design 1

Level	$S^* = 1$ M_n , kN-m (k-ft)	$S^* = 1.2$ M_n , kN-m (k-ft)	$S^* = 1.5$ M_n , kN-m (k-ft)
4-story building			
Floor 2-R†	984 (726)	1180 (870)	1475 (1088)
8-story building			
Floor 5-R	987 (728)	1184 (873)	1480 (1092)
Floor 2-4	1364 (1006)	1636 (1207)	2045 (1508)
12-story building			
Floor 9-R	922 (680)	1106 (816)	1383 (1020)
Floor 5-8	1379 (1017)	1654 (1220)	2068 (1525)
Floor 2-4	1826 (1347)	2191 (1616)	2739 (2020)
22-story building			
Floor 19-R	1605 (1183)	1646 (1214)	2057 (1517)
Floor 14-18	2273 (1676)	2331 (1719)	2914 (2149)
Floor 9-13	2802 (2066)	2874 (2119)	3592 (2649)
Floor 5-8	2874 (2119)	2947 (2174)	3684 (2717)
Floor 2-4	2861 (2110)	2934 (2164)	3668 (2705)

* Variable corresponds to the site coefficient used in the UBC (ICBO [1994]) Eq. 28-2
† "Floor 2-R" refers to those beams at the second level through those at the roof level

Table 2(b)—Prototype beam moments: Design 2

Level	$S^* = 1$ M_n , kN-m (k-ft)	$S^* = 1.2$ M_n , kN-m (k-ft)	$S^* = 1.5$ M_n , kN-m (k-ft)
4-story building			
Floor 2-R†	1608 (1186)	1931 (1424)	2414 (1780)
8-story building			
Floor 6-R	1683 (1241)	2019 (1489)	2524 (1861)
Floor 2-5	2269 (1673)	2723 (2008)	3404 (2510)
12-story building			
Floor 10-R	1622 (1196)	1946 (1435)	2433 (1794)
Floor 6-9	2465 (1818)	2959 (2182)	3698 (2727)
Floor 2-5	2791 (2058)	3349 (2470)	4186 (3087)
22-story building			
Floor 18-R	2399 (1769)	2446 (1804)	3056 (2254)
Floor 14-17	3267 (2409)	3303 (2456)	4164 (3071)
Floor 10-13	3894 (2872)	3972 (2929)	4964 (3661)
Floor 6-9	4282 (3158)	4368 (3221)	5459 (4026)
Floor 2-5	4433 (3269)	4521 (3334)	5651 (4167)

* Variable corresponds to the site coefficient used in the UBC (ICBO [1994]) Eq. 28-2
† "Floor 2-R" refers to those beams at the second level through those at the roof level

tude between the experimental specimen and the design prototype.

The above procedure was used to obtain $M-\phi$ curves for each type of connection. The different types of connections were based on the M_s/M_p ratios where M_s is the moment contribution from the mild steel to the total moment and M_p is the plastic or ultimate moment of the connection. The M_s/M_p ratios used were 0, 0.28, 0.35, 0.45, and 1.00 where a value of zero corresponded to a connection which contained only PT steel with no mild steel and a value of 1.0 corresponded to a monolithic connection which contained only mild steel. The ratio of 0.45 corresponds to the hybrid connection OPZ4.

Choice of accelerograms

A suite of 29 acceleration records from four different earthquakes was used for the input motion in the dynamic analyses. Ten records each from recording instruments situated on the UBC soil types S1 and S3 and nine records for UBC soil type S2 were included in the evaluation. These records were scaled in magnitude (PGA) such that the acceleration response spectra were similar to the UBC design spectra in a specified period range for each of the different soil types. The scale factor was determined by minimizing the error between the scaled spectra and the UBC spectra for periods between 0.4 s (\approx 4 stories) to 2.2 s (\approx 22 stories). The acceleration records used in the present analysis are shown

Table 3—Earthquake records

Recording station name	Earthquake name*	Epicentral distance, km	UBC soil type	Scale factor†	Scaled peak acc., g
1. Caltech Seismic Lab	San Fernando	34	1	2.9	0.555
2. Castaic, Old Ridge Rte.	Whittier	69	1	4.8	0.327
3. Corralitos, 1473 Eureka Canyon Rd.	Loma Prieta	7	1	0.6	0.363
4. Gilroy No. 1, Gavilan College	Loma Prieta	29	1	1.8	0.787
5. Griffith Park Office	San Fernando	33	1	1.8	0.308
6. Pacoima, Kagel Canyon	Whittier	38	1	4.4	0.676
7. Pacoima Dam	San Fernando	8	1	0.5	0.506
8. Santa Cruz, UCSC/Lick Lab	Loma Prieta	16	1	1.6	0.702
9. Superstition Mountain	Imperial	58	1	1.9	0.376
10. Garvey Reservoir	Whittier	3	1	1.6	0.589
11. 8244 Orion Blvd., LA	San Fernando	20	2	1.4	0.364
12. 900 S. Fremont, Alhambra	Whittier	7.3	2	4	0.457
13. Caltech Athenaeum	San Fernando	37	2	3.4	0.374
14. Caltech JPL	San Fernando	29	2	4.7	0.664
15. Caltech Milikan Library	San Fernando	37	2	2.9	0.535
16. Hollywood Storage Bldg., LA	Whittier	24	2	3.3	0.346
17. Hollywood Storage P.E. Lot, LA	San Fernando	36	2	3.5	0.736
18. Palmdale Fire Station	San Fernando	33	2	3.8	0.425
19. Pumping Plant, Pear Blossom	San Fernando	48	2	10	0.933
20. El Centro Array No. 3	Imperial	26	3	1.2	0.434
21. El Centro Array No. 2	Imperial	26	3	1.7	0.464
22. 288 Vernon, CMD Bldg.	San Fernando	49	3	4.8	0.512
23. 4814 Loma Vista, CMD Bldg.	Whittier	13	3	2.9	0.713
24. El Centro Array No. 1, Dogwood Rd.	Imperial	26	3	1.7	0.502
25. Gilroy Array Station No. 2	Loma Prieta	23	3	1.9	0.626
26. El Centro Array No. 5, James Rd.	Imperial	28	3	1.7	0.921
27. Outer Harbor Wharf, Oakland	Loma Prieta	98	3	1.5	0.434
28. San Francisco International Airport	Loma Prieta	24	3	1.7	0.569
29. Naval Base Fire Station, Treasure Island	Loma Prieta	111	3	3.5	0.349

* Moment magnitudes: Imperial Valley (1979) = 7; Loma Prieta (1989) = 7; San Fernando (1971) = 6.6; Whittier (1987) = 6.1
 † Acceleration records were scaled by this factor in the dynamic analyses

in Table 3. A plot of the scaled normalized response spectra for a set of acceleration records for soil type S1 is shown in Fig. 4 along with the UBC design spectrum. Similar suites were constructed for soil types S2 and S3.

DISCUSSION OF RESULTS

As indicated previously, four different building configurations (4, 8, 12, and 22-story frame structures) and two separate designs (beam and column moments and cross section dimensions) were considered. One set was calculated by the authors (Design 1) and the other by a design firm based in California (Design 2). Each frame was modeled with five different connection types representing the range of M_s/M_p ratios tested in the experimental phase of this research, and whose hysteretic characteristics are listed in Table 1. This represents a total of 20 frames, each of which was subjected to a series of 29 recorded earthquake motions given in Table 3. Separate studies were conducted on the effect of varying the hysteretic parameters by ± 20 percent on selected frames. The corresponding change in drift demand was less than ± 20 percent. Hence, the results presented in this section may be viewed as the mean response of five different sets of hysteretic parameters which account for some degree of uncertainty in

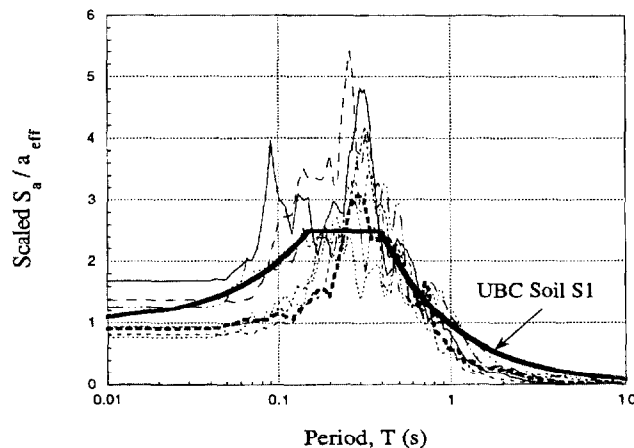


Fig. 4—Normalized response spectra for typical earthquakes used in parametric study

measured concrete properties and observed hysteretic behavior of the prototype connections.

Pushover analysis

Each building model, monolithic and hybrid (Specimen OPZ4), was first analyzed statically under a code-specified

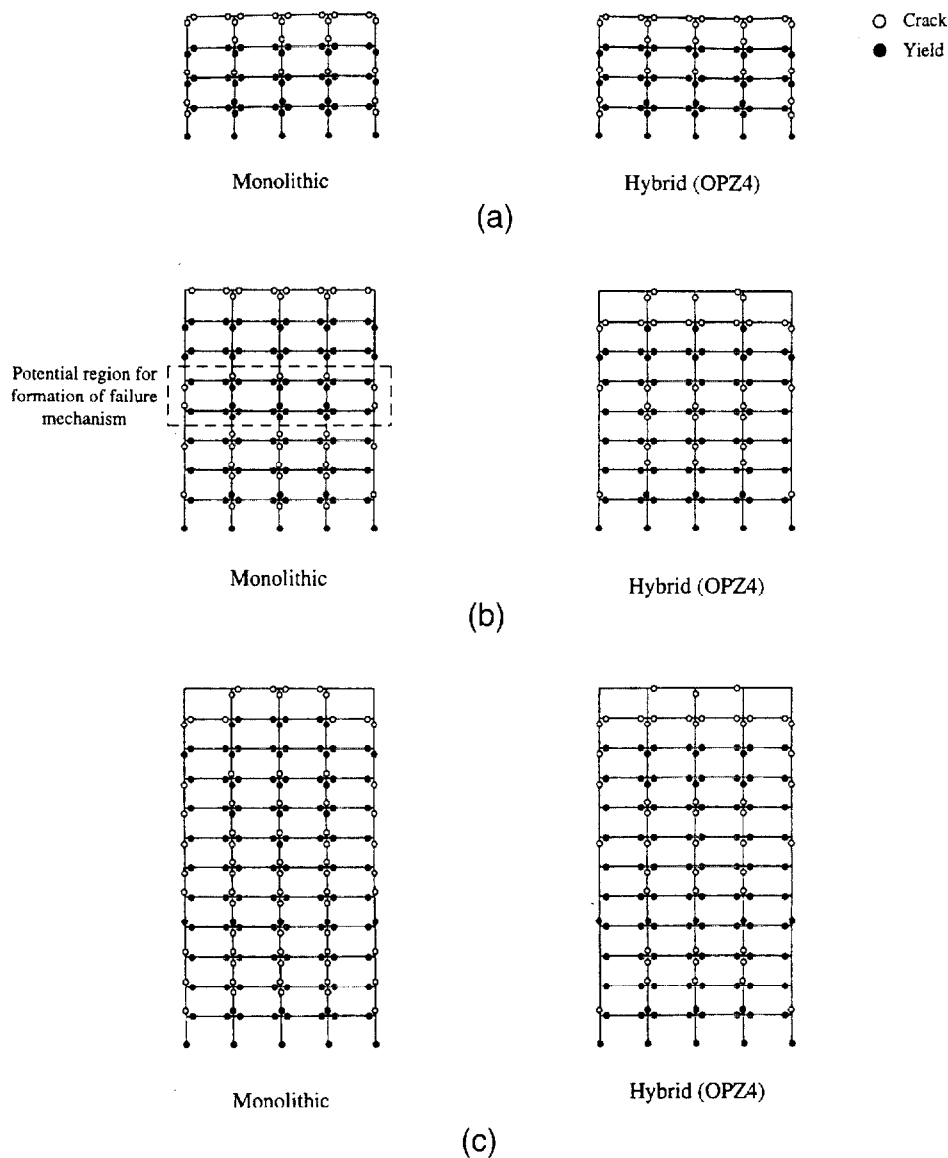


Fig. 5—Failure modes for pushover analyses: (a) 4-story; (b) 8-story; and (c) 12-story

inverted triangular load applied laterally over the height of the building. The inverted triangular load, based on the shear distribution suggested in UBC, was applied incrementally in a monotonically increasing manner until a mechanism was formed and building failure was imminent. Results of the evaluation are presented in Fig. 5(a) through (d) which show the final beam and column hinges. It is observed that some potential exists for mid-story mechanisms to occur in the eight-story building and for lower-story mechanisms to occur in the 22-story building with monolithic connections. As seen in Fig. 5, this potential does not exist for the models with the hybrid connections. The base shears at failure for both types of models (monolithic and hybrid) were similar in these analyses. In general, the performance of the frame with hybrid connections is similar to or better than the corresponding frame with monolithic connections.

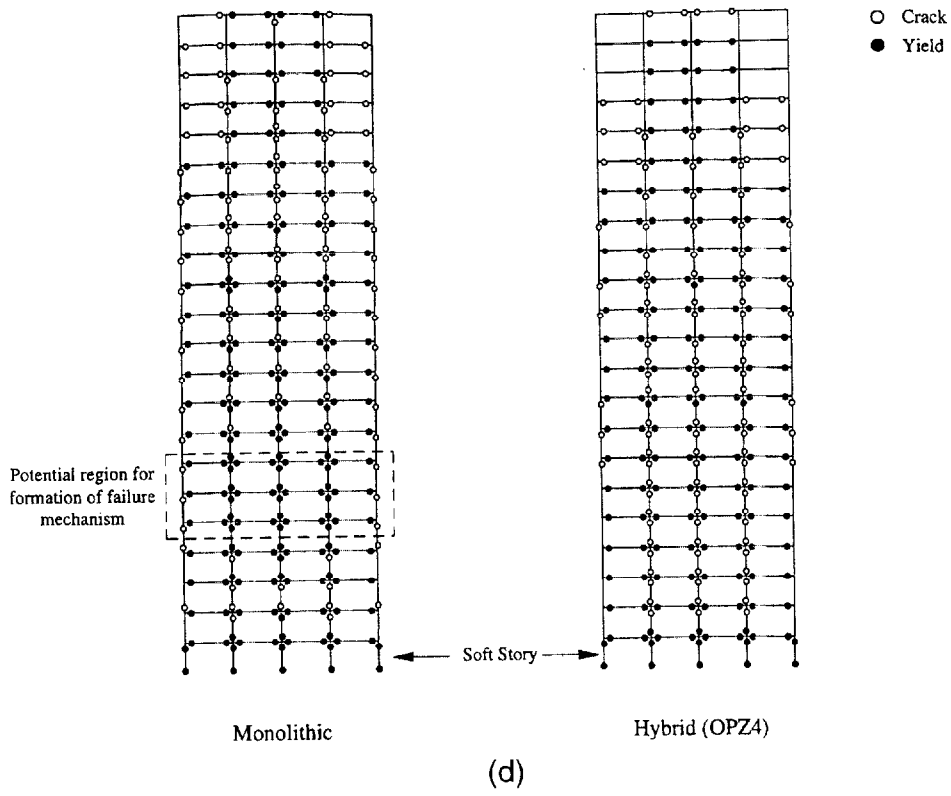
Nonlinear time-history analysis

Maximum inter-story drifts and displacements were obtained for each soil type as a function of building height (or

period). Ten of the 29 records used in the simulations were for soil type S3. Figures 6(a) through (c) show the maximum displacement profile for the 8-, 12-, and 22-story structures subjected to the most severe earthquake on Soil Type S3 for Design One. It is seen that the behavior of the frame with hybrid connections is not very different from that of the frame with monolithic connections.

The effect of higher modes on the response of the building was found to be minimal for the range of structures evaluated in this study. Figures 7(a) and (b) show the time-history response of four different story levels for a severe (Soil Type S3) earthquake for both the monolithic and hybrid frames (Design One). The frame with hybrid connections exhibits a more stable response with less permanent drift than the same system with monolithic connections.

The mean and median drift demands for all Soil Type S1 models were of the order of 0.5 percent. The standard deviation and variance for the story drift were 0.17 percent and 0.03 percent, respectively. On the other hand, the variations in response for Soil Types S2 and S3 were more significant.



(d)

Fig. 5(d)—Failure modes for pushover analyses: 22-story model

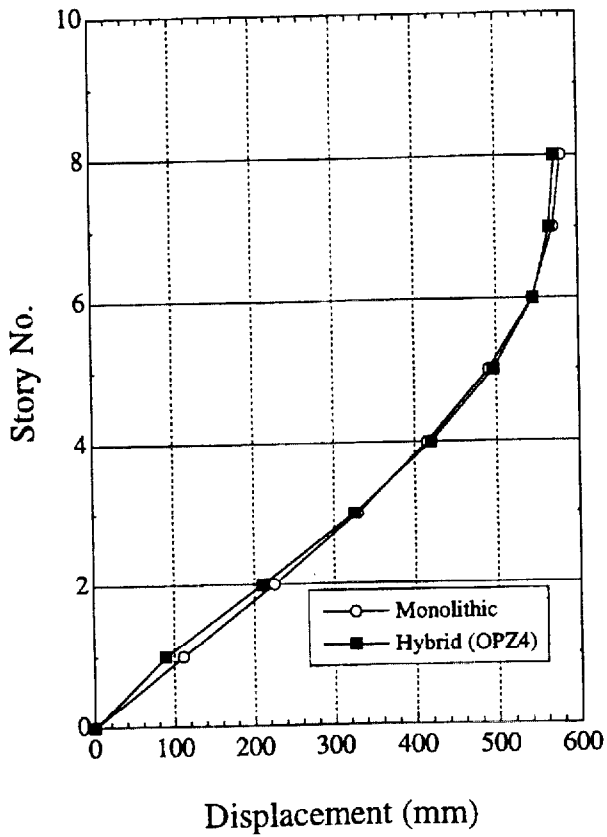


Fig. 6(a)—Maximum displacement profile for most severe earthquake (Soil Type S3): 8-story model

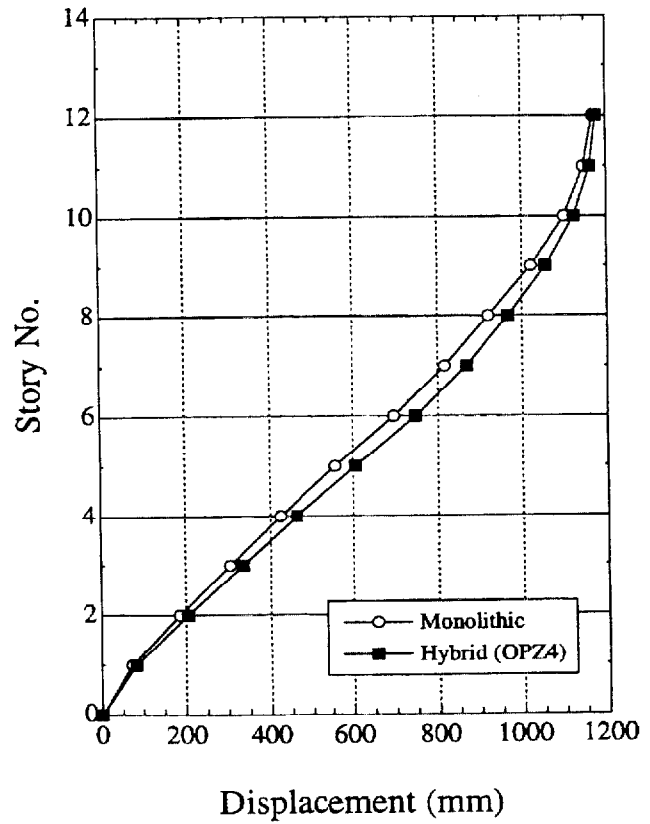


Fig. 6(b)—Maximum displacement profile for most severe earthquake (Soil Type S3): 12-story model

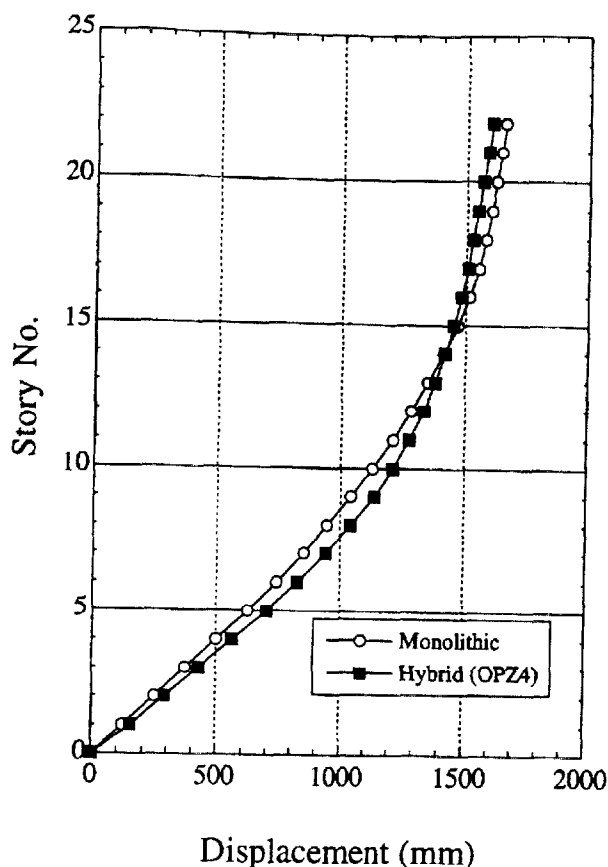


Fig. 6(c)—Maximum displacement profile for most severe earthquake (Soil Type S3): 22-story model

The mean and median drift demands for Soil Type S2 were 1.27 percent and 1.11 percent with a standard deviation of 0.81 percent and a variance of 0.65 percent. Similarly, the mean and median drift demands for Soil Type S3 were 1.93 percent and 1.69 percent with a standard deviation of 0.91 percent and a variance of 0.84 percent. Figures 8(a) through (c) show the drift demand for all frames evaluated in the study. The results are presented by soil type. As expected, the drift demand is highest for S3 soil and the lowest for S1 soil. Also, little difference was found in the drift demand for each of the connection types (precast vs. monolithic) investigated in this study (Cheok et al. [1996]). The scatter associated with connection type is negligible when compared to the scatter associated with a seismic event. Though only four types of frames were considered in the analysis, Fig. 8 shows eight periods; this is a result of using two different designs. The maximum expected drift demands shown in the figures are based conservatively on enveloping approximately 95 percent of the observed peak drift values at all story levels. These drift demands, 3.5 to 4 percent, are higher than that for frames designed per UBC (1994) but they have been found to be more representative of the upper bound of expected inelastic drifts (Uang and Maarouf [1993]; Veletsos and Newmark [1960]).

OBSERVATIONS AND CONCLUSIONS

An important observation from the simulations was that all connections, irrespective of M_s/M_p ratio, produced very sim-

ilar drift demands for both designs. Hence, it may be stated that connections with slightly more energy dissipation capacity fared almost as well as those with less energy dissipation capacity. As seen in Fig. 8, the drift demand appears to be more dependent on the soil type and the acceleration record.

The experimental phase of this investigation provided basic information on the behavior and drift capacity of precast hybrid connections. The observed force-deformation behavior served as the basis for the analytical modeling of precast concrete frames with different hybrid connections. A parametric study carried out on the seismic response of each frame type yielded maximum interstory drift demands for all building types. The computed drift demands appear to be within the limits of experimentally observed behavior for the connections.

In conclusion, the analyses show that the seismic responses of precast concrete frames with hybrid connections are similar to or better than the seismic response of concrete frames with monolithic connections in terms of drift demands and failure modes. The effects of story drift demands in the range of 4 percent on nonstructural elements and building contents is beyond the scope of this paper.

FUTURE RESEARCH

The consequence of excessive drift in terms of P-delta effects requires further investigation which would include a progressive damage analysis of the structure. Also, in the present study, the moment-curvature envelopes for cross-sections were developed from empirical procedures. An enhanced procedure to generate these curves *a priori* for hybrid precast concrete connections, such as those presented in this study, is urgently needed.

ACKNOWLEDGMENTS

The assistance of Suzanne Nakaki, SE, of Englekirk and Nakaki, Inc., Irvine, CA, in providing the designs for the prototype structures is greatly appreciated.

REFERENCES

- Cheok, G. S., and Lew, H. S., "Performance of Precast Concrete Beam-to-Column Connections Subject to Cyclic Loads," *PCI Journal*, V. 26, No. 3, Precast/Prestressed Concrete Institute, Chicago, IL, May-June 1991, pp. 56-67.
- Cheok, G. S., and Lew, H. S., "Model Precast Concrete Beam-to-Column Connections Subject to Cyclic Loading," *PCI Journal*, V. 38, No. 4, Precast/Prestressed Concrete Institute, Chicago, IL, Jul.-Aug. 1993, pp. 80-92.
- Cheok, G. S., and Stone, W. C., "Performance of $1/3$ -Scale Model Precast Concrete Beam-Column Connections Subjected to Cyclic Inelastic Loads—Report No. 3," NISTIR 5246, National Institute of Standards and Technology, Gaithersburg, Aug. 1993.
- Cheok, G. S., and Stone, W. C., "Performance of $1/3$ -Scale Model Precast Concrete Beam-Column Connections Subjected to Cyclic Inelastic Loads—Report No. 4," NISTIR 5436, National Institute of Standards and Technology, Gaithersburg, June 1994.
- Cheok, G. S.; Stone, W. C.; and Nakaki, S. D., "Simplified Design Procedure for Hybrid Precast Concrete Connections," NISTIR 5765, National Institute of Standards and Technology, Gaithersburg, Feb. 1996.
- French, C. W.; Hafner, M.; and Jayashankar, V., "Connections Between Precast Elements Failure Within Connection Region," *ASCE Journal of Structural Engineering*, V. 115, No. 12, Dec. 1989, pp. 3171-3192.
- French, C. W.; Olanrewaju, A.; and Charbel, T., "Connections between Precast Elements—Failure Outside Connection Region," *ASCE Journal of Structural Engineering*, V. 115, No. 2, Feb. 1989, pp. 316-340.
- International Conference of Building Officials, "Uniform Building

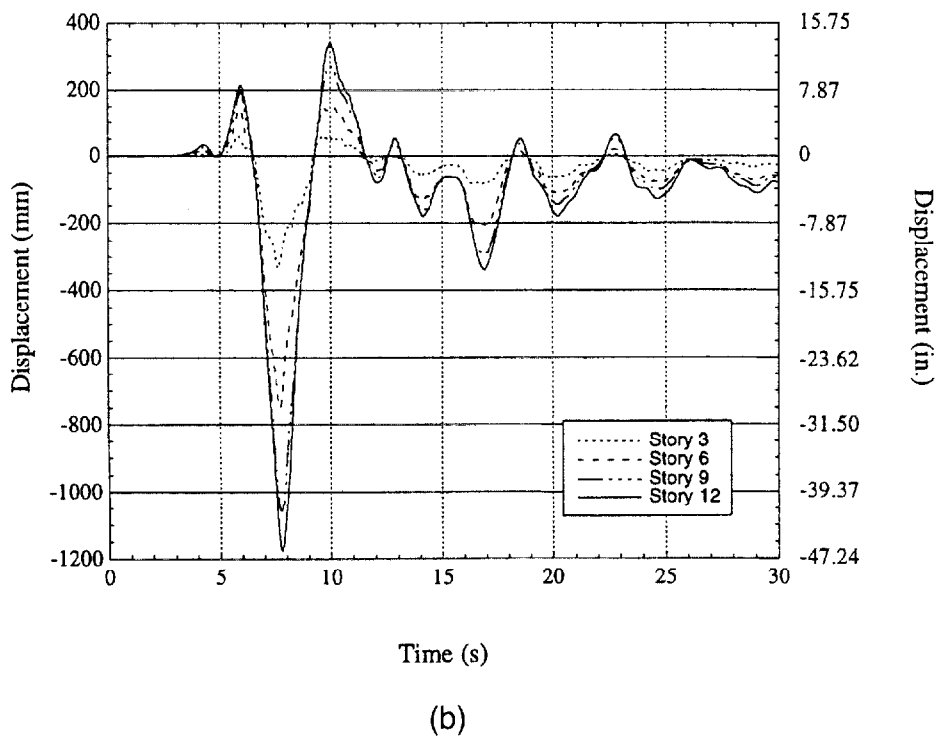
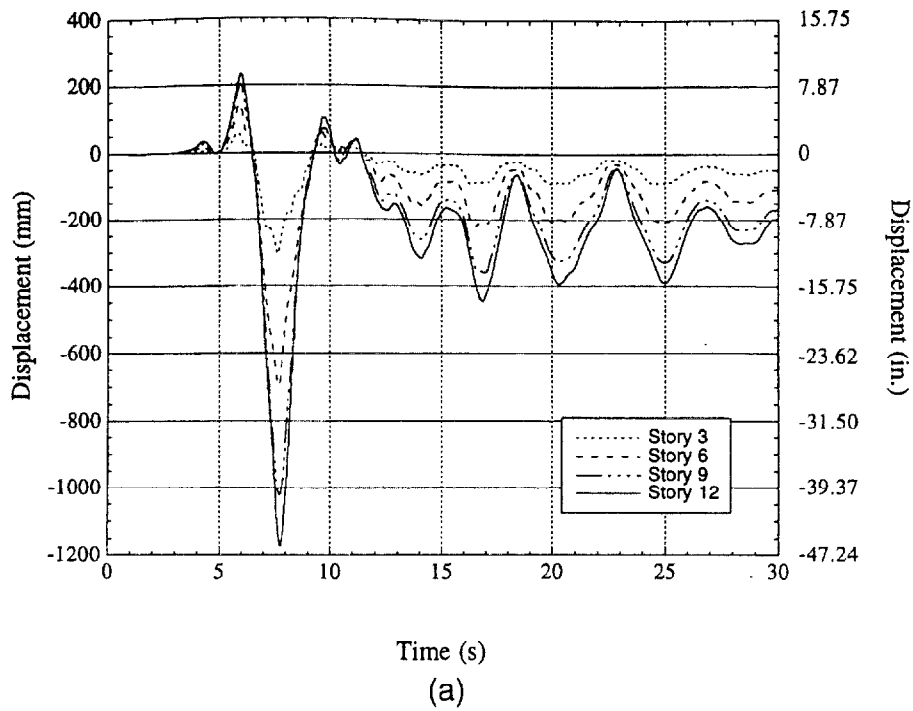


Fig. 7—Response history for 12-story models, Soil S3: (a) Monolithic; and (b) Hybrid

Code: Volume 2, Structural Engineering Design Provisions," Whittier, CA, May, 1994.

Kunnath, S. K.; Reinhorn, A. M.; and Lobo, R. F., "IDARC Version 3.0: A Program for the Inelastic Damage Analysis of Reinforced Concrete Structures." *Technical Report* NCEER-92-0022, National Center for Earthquake Engineering Research, State University of New York at Buffalo, Aug. 1992.

Kunnath, S. K., and Reinhorn, A. M., "Efficient Modeling Scheme for

Transient Analysis of Inelastic RC Structures," *Microcomputers in Civil Engineering*, V. 10, pp. 97-110.

Priestley, M. J. N., ed., "Fourth Meeting of the U.S.-Japan Joint Technical Coordinating Committee on Precast Seismic Structural Systems [PRESSSS]." *Report No.* PRESSSS-94/03, University of California, San Diego, May 1994.

Stone, W. C.; Cheok, G. S.; and Stanton, J. F., "Performance of Hybrid Moment-Resisting Precast Beam-Column Concrete Connections Subjected

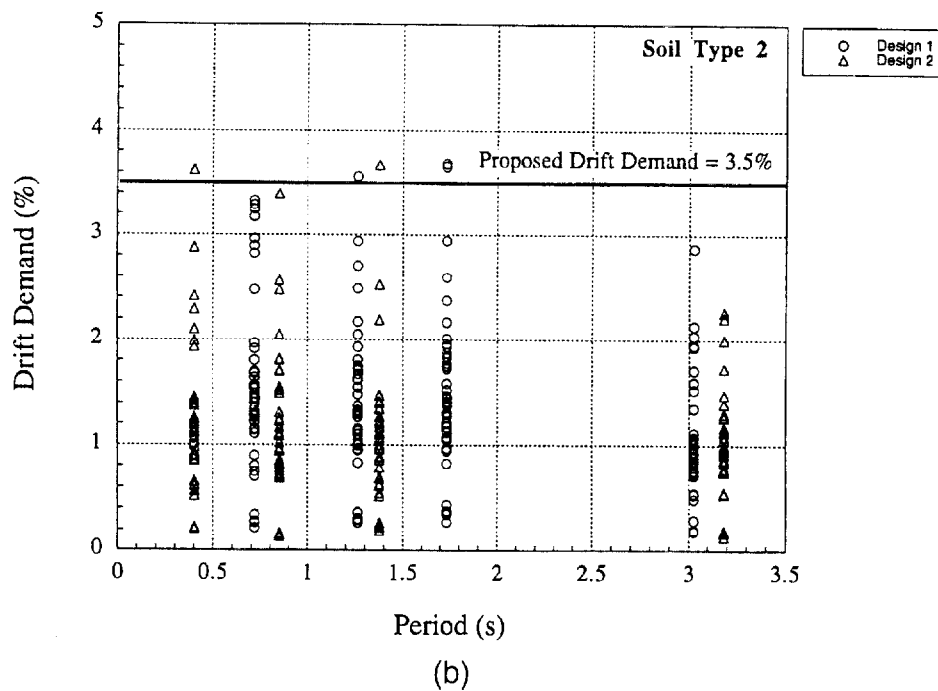
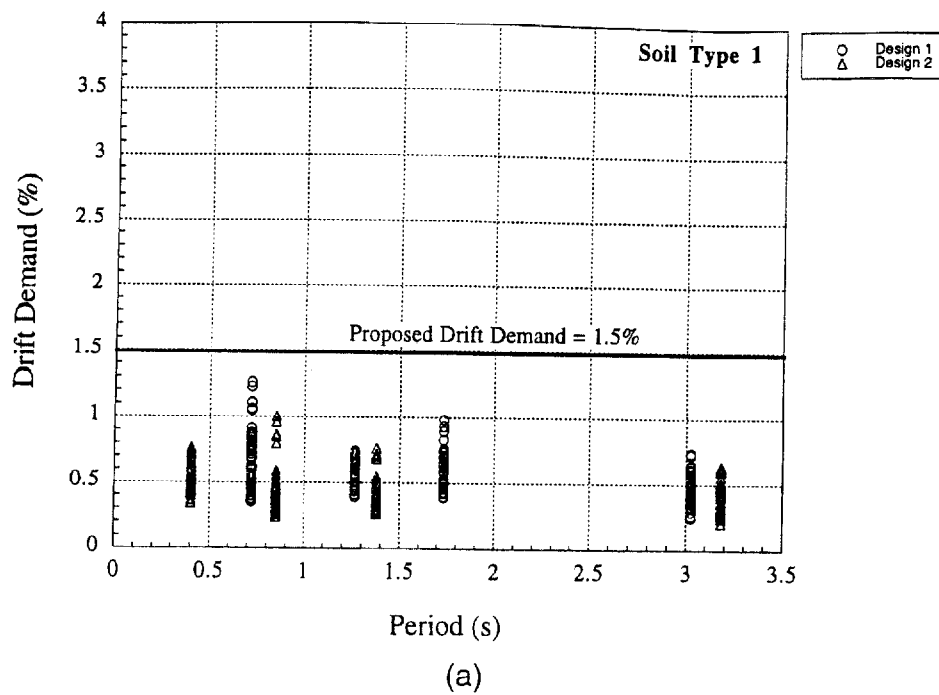


Fig. 8—Drift demand for all models: (a) UBC Soil Type 1; and (b) UBC Soil Type 2

to Cyclic Loading," *ACI Structural Journal*, V. 92, No. 2, Farmington Hills, Mar.-Apr. 1995, pp. 229-249.

Uang, C.-M., and Maarouf, A., "Seismic Displacement Amplification Factor in Uniform Building Code," *SEAOCNC Research Bulletin Board*, BB93-3, June, pp. B1-B2, and "Displacement Amplification Factor for

Seismic Design Provisions," *Proceedings, Structures Congress, ASCE*, V. 1, Irvine, 1993, pp. 211-216.

Veletsos, A. S., and Newmark, N. M., "Effects of Inelastic Behavior on the Response of Simple Systems to Earthquake Motions," *Proceedings, 2WCEE*, Tokyo, Japan, V. 2, 1960, pp. 895-912.

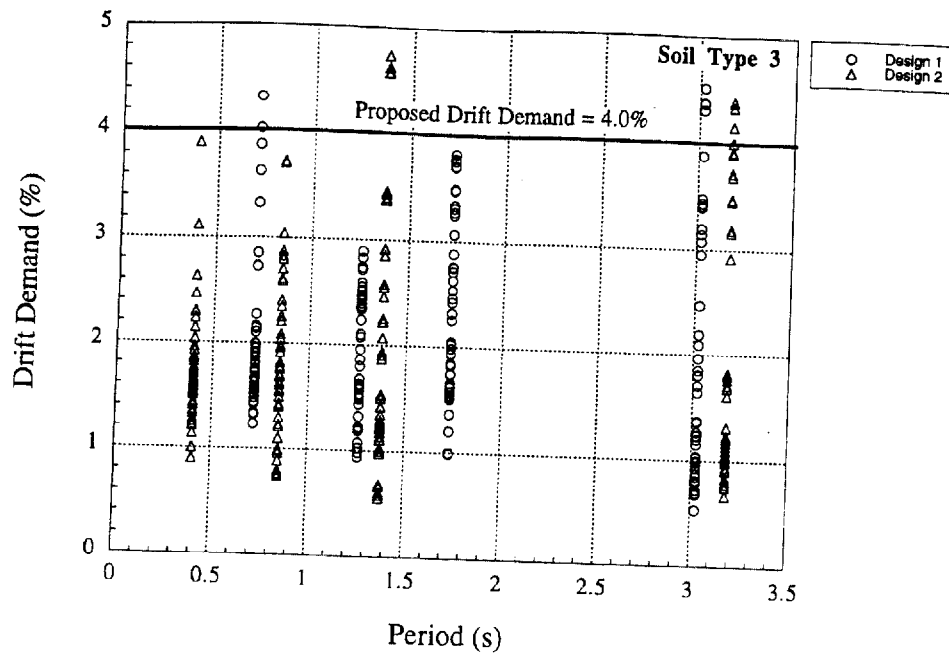


Fig. 8(c)—Drift demand for all models: UBC Soil Type 3